6-22-2004

An Experimental Study of Micron-scale Droplet Aerosols Produced via Ultrasonic Atomization

Thomas D. Donnelly
Harvey Mudd College

J. Hogan '03
Harvey Mudd College

A. Mugler '04
Harvey Mudd College

N. Schommer '04
Harvey Mudd College

M. Schubmehl '02
Harvey Mudd College

See next page for additional authors

Authors
Thomas D. Donnelly, J. Hogan '03, A. Mugler '04, N. Schommer '04, M. Schubmehl '02, Andrew J. Bernoff, and B. Forrest '02

An experimental study of micron-scale droplet aerosols produced via ultrasonic atomization

T. D. Donnelly,[a] J. Hogan, A. Mugler, N. Schommer, and M. Schubmehl
Department of Physics, Harvey Mudd College, Claremont, California 91711

Andrew J. Bernoff[b] and B. Forrest
Department of Mathematics, Harvey Mudd College, Claremont, California 91711

(Received 25 November 2003; accepted 14 April 2004; published online 22 June 2004)

In the last 10 years, laser-driven fusion experiments performed on atomic clusters of deuterium have shown a surprisingly high neutron yield per joule of input laser energy. Results indicate that the optimal cluster size for maximizing fusion events should be in the 0.01–1 μm diameter range, but an appropriate source of droplets of this size does not exist. In an attempt to meet this need, we use ultrasonic atomization to generate micron-scale droplet aerosols of high average density, and we have developed and refined a reliable droplet sizing technique based on Mie scattering. Harmonic excitation of the fluid in the MHz range yields an aerosol of droplets with diameters of a few microns. The droplet diameter distribution is well-peaked and the relationship between average droplet size and forcing frequency follows an inviscid scaling law, predictable by dimensional analysis and consistent with the linear theory for Faraday excitation of an infinitely deep fluid. © *2004 American Institute of Physics.* [DOI: 10.1063/1.1759271]

I. INTRODUCTION

One of the most prominent branches of modern fusion research is inertial confinement fusion (ICF). ICF experiments involve the simultaneous firing of multiple high-intensity laser pulses at a small stationary target. Typically, the targets in these experiments are pea-sized pellets of deuterium. The incident laser pulses implode the pellet, resulting in high temperatures and pressures. In order for nuclear fusion to occur, the pellet temperature must be raised to over 100 000 000 °C, and the density must be increased to more than 1000 times normal solid density.[1] Typically, large-scale lasers are needed to generate the high-intensity pulses required to achieve these temperatures and pressures. For example, the National Ignition Facility, currently under construction, is a 192-beam 2 MJ laser system.[2]

Recent research has demonstrated that 50 Å clusters of deuterium can be used in conjunction with significantly down-sized laser systems to initiate fusion.[3–5] These experiments show that with deuterium clusters as small as 25 Å fusion can be achieved, and that larger clusters correlate with improved neutron yield. However, the gas jets used to produce the clusters cannot generate clusters greater than approximately 50 Å in size. More recently, similar experiments done with 1.0 μm diam droplets have produced copious hard x rays, but no evidence of fusion.[6]

Currently, both experiments and models indicate that the optimum droplet diameter for fusion is in the 0.01–1 μm range, depending to some degree on whether energy is given to ions predominately through Coulombic explosion or hydrodynamic explosion of the target.[7] It is well known that single droplets in this size range can be produced using, for example, electrospray techniques, however, in the relevant fusion experiments, droplets must be produced such that the average atomic density in the focal volume of the laser is approximately atmospheric. To our knowledge, submicron droplets in these quantities have not been previously produced.

In this paper we investigate ultrasonic atomization as a possible method for generating large volumes of droplets in this size range. This method will require that we abandon the use of a pure deuterium source. Instead, a liquid is required, and our studies use water and glycerin with the understanding that heavy water will be used for the actual fusion experiments.

We have used ultrasonic atomization to produce a high-density, relatively monodisperse aerosol of water droplets with an average droplet diameter of ≈ 2 μm. These droplets are generated by driving the fluid harmonically in the MHz frequency range. The droplet sizes follow an inviscid scaling law predictable with dimensional analysis and consistent with the linear theory for capillary waves generated via Faraday excitation.[8–11] Curiously our measured droplet size follows the inviscid scaling up to a critical dimensionless frequecy that is more than 4 orders of magnitude larger than the observed transition to viscous effects in previous work;[12] this disparity appears to be due to the fact that the previous work measured the forcing threshold for droplet ejection whereas we measure droplet size. This point is discussed in more detail in both Secs. II and IV.

Currently, we produce droplets using a piezoelectric oscillator. The oscillator is placed at the bottom of several centimeters of fluid and is then driven at 1–2 MHz; this results in the production of a fine aerosol. Droplet diameters are

[a]Electronic mail: tom_donnelly@hmc.edu
[b]Electronic mail: ajb@hmc.edu

then determined using the technique of Mie scattering.[13] This entails directing a laser through the aerosol and measuring the angular scattering pattern that is produced and then using Mie theory to infer a droplet size distribution. Comparisons with hydrodynamic scaling arguments and linear theory for the Faraday instability of an infinitely deep fluid predict how the droplet diameter should scale with driving frequency, viscosity, density, and surface tension of the sample fluid. By varying these parameters, we can control droplet size, suggesting that this technique should be useful in building a droplet source for fusion research.

II. THEORY

The experiment is modelled as a harmonically driven viscous, incompressible fluid, classically known as Faraday excitation (for a review see Ref. 14). The droplet sizes and characteristic wavelengths are so small (typically 1 μm in size) that the fluid is effectively infinitely deep and infinitely wide (the cylindrical container in which we drive our fluids is 10 cm in diameter and filled to a depth of 6 cm), with a free boundary at the surface on which the viscous stresses must balance the forces due to surface tension and pressure. We first consider the problem via dimensional analysis, and then refine our predictions using linear theory for viscous Faraday excitation and making the assumption that the diameter of the droplet ejected should be proportional to the most unstable wavelength of excitations of the free surface.

A. Faraday excitation

Since Faraday observed his eponymous excitation of a fluid surface in 1831,[15] the study of parametrically driven free surface waves has been an active field of study. In 1954, Benjamin and Ursell[16] showed that Faraday excitation could be modeled with the Mathieu equation; they studied linear theory for the inviscid problem and incorporated viscosity as a weak perturbation. Their work provided a solid underpinning to the fact that the initial instability of the fluid is subharmonic; that is waves with an oscillation frequency of half the forcing frequency are most easily excited. Miles and Henderson[14] review earlier literature on this problem, which generally concentrated on cases when viscosity leads to weak dissipation in the inviscid problem.

In the past decade analysis of the linear stability of the full viscous problem has become both computationally feasible and experimentally relevant. Kumar and Tuckerman[17] considered linear stability of viscous excitation of two fluids layers; they reduced calculation of the neutral stability curves to finding when there is a solution for a temporal Fourier series. Truncation of this series yields a straightforward linear algebra problem. They obtain good agreement with experiments on the onset of instability in viscous fluids. We will adopt their methods below. Beyer[18] also solved the full viscous problem numerically, and with an arbitrary forcing function. Bechhoefer *et al.*[19] compared experiments to viscous theory using the methods of Kumar and Tuckerman accounted heuristically for the effects of a finite-sized container.

While the dependence of the threshold amplitude and most unstable wavenumber at onset on the forcing frequency in the presence of weak dissipation was understood in the 1950s by Benjamin and Ursell, the relationship in the highly dissipative limit only became of interest in the last decade, driven by the availability of highly accurate experimental data. In 1997, Lioubashevski *et al.*[20] suggested that in the highly dissipative limit the instability is governed by a Rayleigh–Taylor instability; physically they noted that for half the oscillation the fluid is accelerating downward, leading to instability of the fluid surface. For shallow containers, they showed the scaling behavior at onset was independent of surface tension. Cerda and Tirapegui[21,22] investigated asymptotically the behavior of the viscous Faraday problem, and derived scalings for the onset behavior in a variety of cases, including the highly dissipative case. Kumar[23] compared calculations of the Faraday instability and the Rayleigh–Taylor instability, using a mean-field approximation for the acceleration. He concluded that the Rayleigh–Taylor approximation was valid in the limit of large depth.

Miles[24] formulated the linear stability problem for Faraday excitation in an infinitely deep and infinitely wide fluid in terms of the impedance of the liquid. He develops expressions for the growth rate of the instability as an expansion in coupling to the harmonics of the forcing frequency. Among other useful expressions, Miles develops an approximation for the most unstable wave number in the limit of large viscosity, which is dimensionally consistent with the previous works but also includes an analytical calculation of the constant of proportionality which we verify numerically.

The idea that the size of droplets ejected is related to the most unstable capillary wavelength goes back to at least Lang[10] in the early 1960s, who cleverly measured the size of droplets of molten wax that were ejected (and subsequently solidified). More recently, the constant relating droplet diameter to wavelength has been measured for waves of thin films by Dobre, Bolle, and Sindayihebura.[8,11] With improved particle sizing techniques using Mie scattering, we determine this constant experimentally with greater precision than previously possible.

The relationship of droplet ejection to the amplitude of the applied forcing was studied extensively in the experiments of Goodridge *et al.*,[12,25] who studied water and water/glycerin mixtures forced at frequencies up to 100 Hz. They showed that at low frequencies the critical forcing amplitude for ejection followed an inviscid scaling and that as the frequency was increased a transition to a viscously dominated regime was seen. They deduced the scaling behavior of the threshold amplitude with forcing frequency via dimensional analysis and verified these scalings analytically. We use similar arguments to deduce the dependence of droplet diameter in this paper; the one curious variance between their work and ours is that the viscous effects on the threshold acceleration for ejection become evident 4 orders of magnitude below where we observe inviscid scaling in the droplet size. A plausible explanation for this can be made by considering the linear stability theory for Faraday waves; viscous effects are a singular perturbation in the threshold amplitude, delaying onset to an amplitude proportional to the viscosity. However,

viscous effects are a regular perturbation of the most unstable wavelength at onset, detuning the inviscid result by an amount proportional to the viscosity. Consequently, we suggest that viscous effects will be more easily observed when considering threshold accelerations, as was the emphasis of the studies of Goodridge *et al.*

More recently, James *et al.*[26,27] considered the atomization of a sessile fluid droplet when being forced by a piezo at ≈ 1000 Hz. They observe a sequence of droplet ejections leading to the atomization of the initial sessile droplet.

In summary, droplet ejection has generally been studied at forcing frequency of 1–1000 Hz; typically we are working at frequencies in the MHz range, producing droplets with diameters a factor of 100 smaller than previous experiments.

B. Dimensional analysis

Consider a fluid with surface tension σ [mass/(time^2)], density ρ [mass/(length)^3], and kinematic viscosity, ν [(length)^2/time] which is displaced vertically by an oscillator a distance $a\cos(\omega t)$. Following Goodridge *et al.*,[12] we nondimensionalize on the fluid parameters; the unique frequency ω_*, lengthscale ℓ_*, and mass m_* that can be constructed are

$$\omega_* = \frac{(\sigma/\rho)^2}{\nu^3}, \qquad \ell_* = \frac{\nu^2}{\sigma/\rho}, \qquad m_* = \rho \ell_*^3. \tag{1}$$

We can then construct a nondimensional forcing amplitude $A = a/\ell_*$ and a nondimensional forcing frequency $\Omega = \omega/\omega_*$. These two control parameters completely specify the nondimensional fluid system.

We can now apply intuition and dimensional analysis to deduce the relationship between the nondimensional droplet diameter, $D = d/\ell_*$ (where d is the dimensional diameter) and the forcing frequency for the inviscid and viscous regimes.

For $\Omega \ll 1 (\omega \ll \omega_*)$, we expect that viscous effects will be negligible and the droplet diameter will be independent of the fluid viscosity. Moreover, if we assume that the droplet diameter is independent of the forcing amplitude, the only possible relationship between D and Ω is

$$D \propto \Omega^{-2/3} \Rightarrow d \propto (\sigma/\rho)^{1/3} \omega^{-2/3}. \tag{2}$$

This agrees with experimental results on droplet size in the literature, and is equivalent to assuming that the droplet size is proportional to the most unstable wavelength in Faraday excitation near onset.[8,10,11]

For $\Omega \gg 1 (\omega \gg \omega_*)$, we expect that viscous effects will dominate and we might hypothesize that the droplet size is independent of the surface tension. If, once again, we assume that the droplet diameter is independent of the forcing amplitude, we conclude

$$D \propto \Omega^{-1/2} \Rightarrow d \propto \nu^{1/2} \omega^{-1/2}. \tag{3}$$

We have again made the questionable assumption that the forcing amplitude plays no role in determining the droplet size. Once again this is equivalent to assuming the droplet size is proportional to the most unstable wavelength in Faraday excitation near onset. While we cannot verify this assumption, we will demonstrate below that surface tension plays no role in determining the most unstable wavelength at the onset of instability in the Faraday problem at large forcing frequencies.

C. Linear stability for the viscous Faraday problem

Following the method of Kumar and Tuckerman,[17] we analyze linear stability for the Faraday excitation of an infinitely deep fluid. We omit most of the details in the derivation below, as they are well documented in the literature.

Plane wave solutions in this problem decouple, so it suffices to consider a two-dimensional fluid. Choose a coordinate system with the x axis parallel to the fluid surface and the z axis perpendicular to the fluid surface. Take the fluid surface at rest to be at $z=0$ and let the fluid occupy the space where $z \leqslant 0$ for all values of x. By shifting into the frame of the oscillator we model the acceleration, $\zeta(t) = a\omega^2 \cos(\omega t)$, as a body force applied to the fluid.

We nondimensionalize with the scales (1) and linearize the governing Navier–Stokes equations, the tangential and normal surface–stress balances, and the kinematic equation. This yields a coupled set of partial differential equations (PDEs) with associated boundary conditions. If we further look for plane wave solutions, we can reduce the problem to a set of PDEs for the surface displacement

$$H = H(T) e^{iKX}, \tag{4}$$

and the vertical velocity

$$W = W(Z,T) e^{iKX}, \tag{5}$$

where K is the nondimensional surface wave number and X, Z, and T are the nondimensional coordinates.

In the bulk of the fluid we satisfy the linearized Navier–Stokes equation; the vorticity equation is

$$(\partial_{ZZ} - K^2)(\Omega \partial_T - \partial_{ZZ} + K^2) W = 0, \quad Z < 0. \tag{6}$$

On the surface ($Z=0$), we must satisfy the normal and tangential force balances,

$$(-3K^2 + \partial_{ZZ} - \Omega \partial_T) W_Z = (K^4 + AK^2\Omega^2 \cos(T)) H, \tag{7}$$

$$(K^2 + \partial_{ZZ}) W = 0, \tag{8}$$

and the kinematic condition

$$\Omega \frac{dH}{dT} = W. \tag{9}$$

Finally we note that the velocity must remain bounded as $Z \to -\infty$.

This system is solved by writing solutions in Floquet form, with the periodic piece of the solution written as a Fourier series in time. Solving for values where periodic solutions exist (that is where the Floquet exponent is 0), yields the neutral stability curves. Again, the reader is referred to

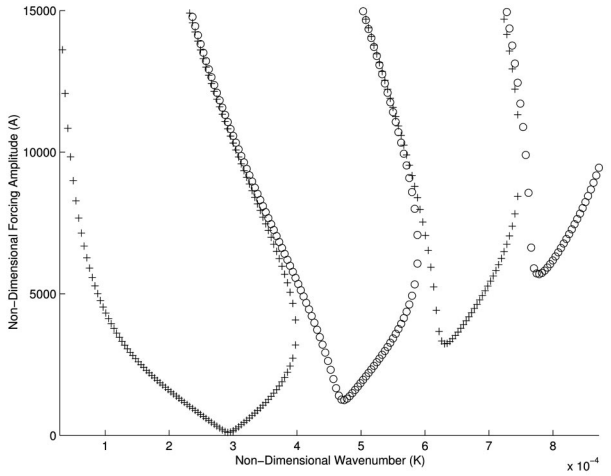

FIG. 1. Plot of A vs K for $\Omega = 10^{-5}$. The plotted points correspond to the neutral stability curves of the full hydrodynamic system. Note that the + symbols correspond to subharmonic solutions, while the ○ symbols correspond to harmonic solutions. The minimum amplitude point on this neutral stability curve is at $(K,A) \approx (2.9\times 10^{-4}, 1.1\times 10^{2})$.

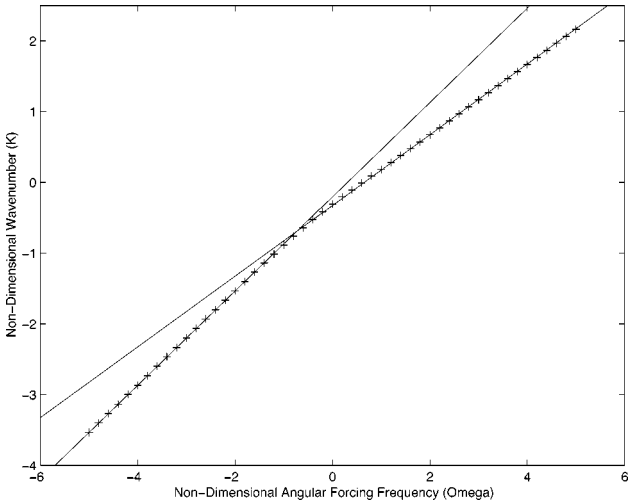

FIG. 3. Log–log plot of wave number vs forcing frequency at threshold. The wave number at the point of minimum amplitude on the neutral stability curves is graphed as a function of the angular forcing frequency. The plot demonstrates two distinct scaling regimes, inviscid for $\Omega > \bar{\Omega}$ and viscous for $\Omega < \bar{\Omega}$, where $\bar{\Omega} \approx 0.1756$ is the crossover point.

the detailed discussion of the numerical solution of this system in Kumar and Tuckerman[17] and the thesis of Forrest[9] which will not be repeated here.

D. Neutral stability curves and scalings

Figures 1 and 2 are the neutral stability curves for the system in the limits of small and large viscosity, respectively. Over a range of Ω from 10^{-5} to 10^{5} these neutral stability curves were examined to find the value of K at the point of minimum A on the neutral stability curve for a given Ω. This K is the most unstable wave number at the onset of the Faraday instability; we will assume that the diameter of the aerosolized droplets is proportional to this wave number. Figure 3 is a log–log plot of wave number as a function of forcing frequency.

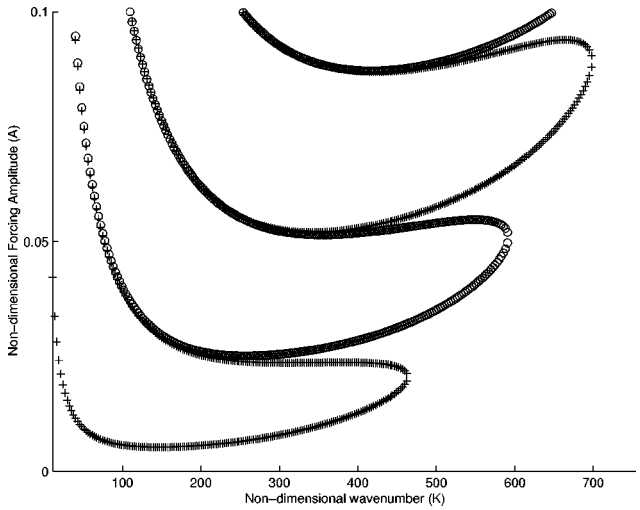

FIG. 2. Plot of A vs K for $\Omega = 10^{5}$. The plotted points correspond to the neutral stability curves of the full hydrodynamic system. Note that the + symbols correspond to subharmonic solutions, while the ○ symbols correspond to harmonic solutions. The minimum amplitude point on this neutral stability curve is at $(K,A) \approx (1.5\times 10^{2}, 5.4\times 10^{-3})$.

Figure 1 is a typical neutral stability diagram for the weakly inviscid Faraday instability, or equivalently the Mathieu equation (cf. Benjamin and Ursell[16] and many others more recently). For $\Omega \ll 1$, we expect the most unstable wavelength to correspond to a capillary wave with the subharmonic frequency

$$(\Omega/2)^2 = K^3 \Rightarrow k = 2^{-2/3}(\sigma/\rho)^{-1/3}\omega^{2/3} \approx 0.6300(\sigma/\rho)^{-1/3}\omega^{2/3}, \tag{10}$$

where the relationship for dimensional k and ω is valid for $\omega \ll \omega_{*}$. In Fig. 3, we see that this relationship certainly fits the linear stability calculation for small Ω. In this inviscid regime, the instability wavelength is independent of viscosity, and depends only upon the ratio of the fluid's surface tension and density. However, we note that viscosity does displace the amplitude of onset of Faraday waves from zero to a finite threshold, proportional to the viscosity.

For $\Omega \gg 1$, our dimensional analysis suggests that Ω is proportional to K^2. In this viscous regime, the relationship between the dimensional k and ω is independent of surface tension and density, and depends only upon viscosity, as might be deduced if we assume the instability is governed by a Rayleigh–Taylor mechanism.[20,23] Miles[24] gives an expression for the most unstable wave number in this case

$$\Omega = \frac{9}{2}K^2 \Rightarrow k = \frac{\sqrt{2}}{3}\sqrt{\frac{\omega}{\nu}} \approx 0.4714\sqrt{\frac{\omega}{\nu}}, \tag{11}$$

which is consistent with our numerics, and is plotted in Fig. 3.

Note that these two asymptotes (10), (11) cross at $\Omega \equiv \bar{\Omega} = 128/729 \approx 0.1756$, which roughly represents the crossover point between the two scaling regimes.

It should be emphasized that this crossover point ($\Omega \approx 0.1756$) represents the transition between the inviscid and viscous regimes with respect to the most unstable wave-

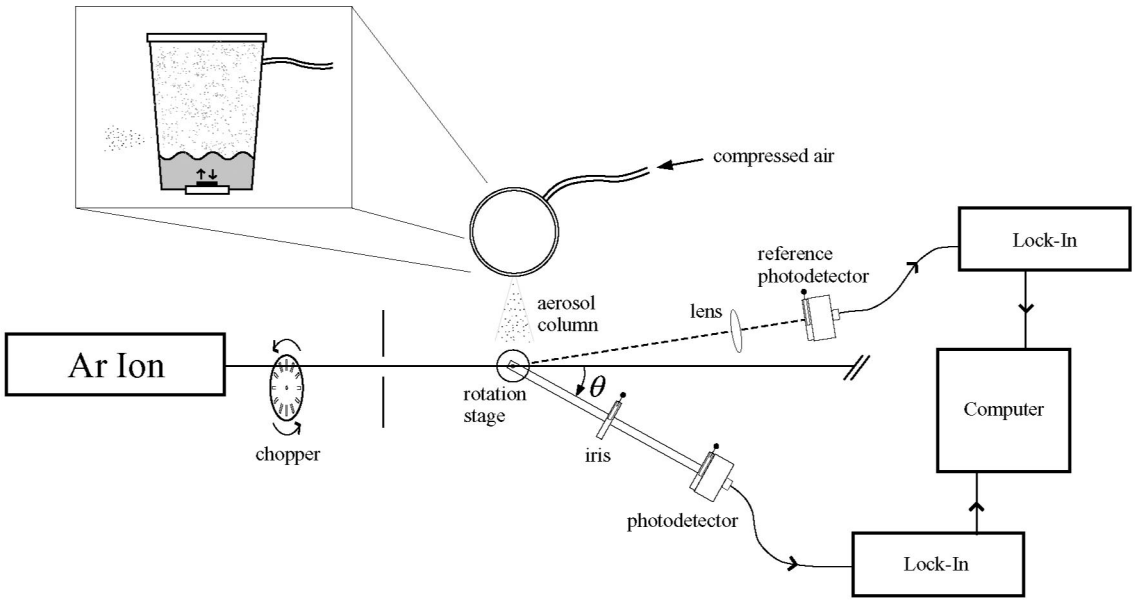

FIG. 4. The experimental setup. Droplets were generated by ultrasonic atomization and were sized using Mie scattering measurements. A reference arm was used to normalize the intensity measured at each angle θ to correct for variations in aerosol density and laser intensity. A 1 W argon ion laser operating at 488 nm was used for the incident beam. The inset figure is a cartoon of the fluid being atomized by the piezo. Note that in the inset a side view of the piezo and fluid is shown, as compared to the top view in the main figure.

length at the onset of instability, which we use as a proxy for droplet size. This contrasts sharply with the results of Goodridge,[12] who measured critical acceleration for droplet ejection and found a crossover at $\Omega \approx 10^{-5}$. This suggests that viscous effects on the threshold ejection amplitude dominate at a much lower frequency than viscous effects on the threshold wavelength. A simple observation that suggests the role of viscosity may be different in these two systems is the fact that in the weakly viscous theory,[14,16,22,24] the threshold for instability is proportional to the viscosity while the threshold wavelength is independent of viscosity at leading order. However, a complete resolution of this discrepancy probably awaits a full numerical study of the nonlinear viscous ejection problem.

III. EXPERIMENT

A. Ultrasonic atomization

Five piezoelectric oscillators with resonant frequencies ranging from 1.52 to 2.42 MHz were used to create the droplets. The driving frequency was controlled by using piezoelectric disks of various thicknesses, each with a different resonance frequency. The piezoelectrics were driven at resonance in order to maximize the driving amplitude. Various glycerin–water solutions were used in order to vary the fluid density ρ, surface tension σ, and kinematic viscosity ν, with concentrations of glycerin ranging from 0% to 60% by weight. This range of fluid parameters and driving frequencies has allowed data to be obtained over roughly 2 decades of nondimensional driving frequency, Ω. We have only recently been able to atomize glycerin solutions with concentrations above 60%, and we hope to report on them in the future.

B. The droplet sizing technique

Droplets were sized using a light scattering technique developed in previous work.[13] A 1 W argon ion laser operating at 488 nm polarized perpendicular to the table was directed through the aerosol. The droplets in the aerosol scatter the laser light in a measurable manner, and the resulting angular scattering intensity pattern is characteristic of the ratio of the droplet size to the incident wavelength. This ratio is called the size parameter, and it is defined as

$$x = \frac{2\pi R}{\lambda}, \tag{12}$$

where R is the droplet radius and λ is the wavelength of the incident light. For each aerosol produced, we measured the angular scattering pattern and then used Mie scattering theory to infer a droplet size. Figure 4 shows the setup used to measure the scattering pattern. Using this technique, we typically size micron scale droplets with a precision of 0.1 μm or better.

To measure the angular scattering pattern, the aerosol was directed over the center of a rotation stage. An amplified photodetector was connected to the rotation stage via a rail, and was positioned 24.5 cm from the center of the stage. The need for an iris on the rail between the center of the rotation stage and the photodetector restricted θ in Fig. 4 to angles larger than 5°. While no physical constraint limited the maximum angle, we found that for angles larger than 30° the signal strength was too small to be accurately resolved. We measured the scattered light intensity at 15 different angles between 6° and 30°, and our angular resolution was 0.5°.

During the course of a single scattering measurement, the density of the mist can fluctuate significantly. This occurs

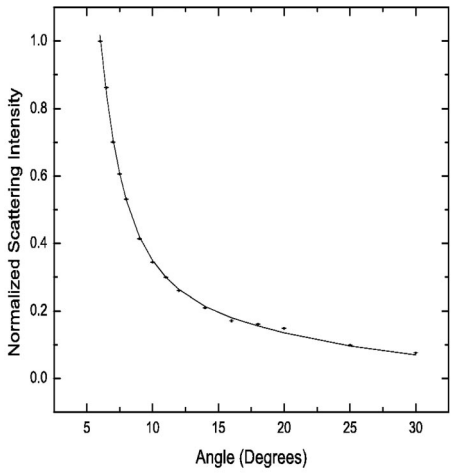

FIG. 5. Mie scattering intensity data. Angular intensity data for one data set is shown. The solid line is a numerical fit which performs the Mie scattering calculations and minimizes χ^2 assuming a lognormal distribution of droplet sizes.

because the compressed air pressure is somewhat variable, and because the piezoelectric aerosol generator is not a continuous source, but rather it erratically produces puffs of aerosol. In order to correct for such variations in aerosol density, the signal from a reference photodetector fixed at $-7°$ was used to normalize the moving detector signal. We found that accurate normalization was very important, primarily because the droplet density of the aerosol varied rapidly over the course of a dataset, causing the absolute signal strength to fluctuate. Since the local density of the aerosol column almost certainly varies with position, the absolute light intensity emanating from a point in the aerosol depends on which point of the aerosol is being viewed. Furthermore, if the reference and signal photodetector are looking at different points in the aerosol during a measurement, then the resulting data point will not be properly normalized. Since it is not feasible to normalize each measurement by the local absolute intensity viewed by the signal detector, we use the average of the absolute intensity over the entire aerosol column. We measured the average absolute light intensity of the aerosol column by using a lens to image the column onto the reference photodetector. By imaging the entire column onto the detector at once, we effectively average over all local variations in intensity, and this guarantees that our normalization signal is a measurement of the absolute light intensity. Normalization by this method has the added advantage of automatically correcting for any variations in incident laser intensity that might occur during a dataset.

The incident beam was chopped, and analog lock-in amplifiers were used to enhance signal detection. These amplifiers are designed to ignore all signals that do not oscillate at the specified chopper frequency, and in this way they eliminate a good deal of noise from the signal.

At each angle, the normalized signal was averaged over a 10 s sampling period with the sampling rate set at 10 scans/s. Although nothing prevented the scan rate from being increased, it was unnecessary to scan more frequently due to temporal averaging by the lock-in amplifiers.

Typical angular intensity data are shown in Fig. 5.

C. The effect of temperature on droplet size

During the atomization process, the fluid temperature was closely monitored and recorded in order to account for the temperature dependence of each of the fluid properties. The average temperature variability over the course of a single droplet sizing dataset was found to be $\delta T = 0.6\,°\mathrm{C}$. We found that over this small temperature range, the properties of the fluids employed are well characterized by the average measured temperature, T_{average}. However, the average temperature often differed significantly between datasets, and the effect that this has on each of the fluid properties cannot be ignored when calculating the nondimensional droplet diameter D and driving frequency Ω. We corrected the fluid properties ρ, σ, and ν based on the observed value of T_{average}. This was done by making temperature interpolations of the available fluid property data and then evaluating these functions at T_{average}. In addition, the small temperature uncertainty δT that we observed during each individual dataset was used to calculate the uncertainties for ρ, σ, and ν. These uncertainties contribute to our reported uncertainty in both D and Ω.

D. Numerical fitting routine

Once the angular scattering pattern was measured, Mie scattering theory was used to infer a droplet size.[13] The intensity data sets such as the one shown in Fig. 5 were numerically fit with the help of a modified version of the Fortran MIEV0 program.[28] This program generates the theoretical Mie scattering intensities that are needed to determine a droplet size. However, the aerosols produced in this experiment are not monodisperse as MIEV0 assumes. The complicated process of droplet ejection, in addition to other processes such as droplet coalescence, results in an aerosol that must be described by a distribution of droplet sizes. When compared to a Dirac or normal distribution, we have found that such polydisperse aerosols are best modeled by a lognormal size distribution. The lognormal distribution is given by

$$n(r) = \frac{1}{\sqrt{2\pi}\sigma r}\exp\left[\frac{(\ln r - \ln \overline{r})^2}{2\sigma^2}\right], \tag{13}$$

where $n(r)$ is the relative abundance of droplets with radius r, $\ln \overline{r}$ is the mean value of $\ln r$, and σ^2 characterizes the variance of the distribution.[29] For our purposes, the lognormal distribution is superior to the normal distribution because it does not permit negative particle sizes, and, although it allows for it, the lognormal distribution does not assume a symmetric distribution about the peak size. This asymmetry is physically significant because it gives us some ability to account for coalescing droplets. Coalesced drops are of particular significance because larger drops scatter much more light than smaller drops (the scatter intensity is nonlinear in size). The lognormal distribution is widely used in the aerosol literature, and we follow this tradition in our analysis.

In order to perform a fit using the lognormal distribution (or any other we might prefer), we approximate the continuous distribution as being made up of a finite number of monodisperse populations, each population with the appropriate weight to simulate the particular distribution we are trying to model. In other words, we discretize the continuous distribution; the discretization is accomplished using a size-parameter step size of 0.02. We then run the MIEV0 code for each individual monodispersed population and sum the scattering intensities from each population to obtain the scattering signal that would result from the entire distribution. We then repeat this procedure for a lognormal distribution with slightly perturbed parameters; the perturbations are determined using a Levenberg–Marquardt algorithm. The best fit is determined when we have minimized χ^2.

For any single distribution, we can determine a numeric uncertainty in our particle size based on a χ^2 analysis. Our program varies the value r from the best fit value, and then refits all other parameters in an attempt to find the minimum χ^2 associated with the new r value. In this way the program calculates the minimum χ^2 as a function of r. Once the functional dependence of χ^2 on r is known, the local curvature of χ^2 about the minimum r value can be used to determine the uncertainty in r. This is found according to[30]

$$\delta r = \sqrt{\frac{2}{\frac{\partial^2(\chi^2)}{\partial r^2}}}, \tag{14}$$

where δr is the uncertainty in r. It is important to note that the uncertainty we state in r is the uncertainty in the value of the distribution's peak, it does not indicate the width of the distribution. Further, this uncertainty does not reflect the full empirical uncertainty of the measurement; this value is determined using a sample variance technique and is described in Sec. IV A.

IV. DATA AND RESULTS

A. Droplet sizing measurement

Droplet diameter measurements were made on 58 different aerosols of water and water–glycerin mixtures of 20%, 40%, and 60% glycerin by weight; the data are shown in Fig. 6. Since each aerosol consists of a distribution of droplet sizes, we used the diameter d_{peak} corresponding to the peak of the lognormal distribution to determine the nondimensional diameter D of each aerosol. The average peak droplet diameter of the 58 aerosols was $\langle d_{\text{peak}} \rangle = 2.74\ \mu$m, with a standard deviation of 0.5 μm. The aerosol with the smallest peak droplet diameter had $d_{\text{peak}} = 2.02 \pm 0.06\ \mu$m, and was made using water with a driving frequency of 2.42 MHz.

The results shown in Fig. 7 are found from measurements made over a period of months. Here we see the distribution of droplets produced by driving pure water at 2.42 MHz. Of all our data, this set shows the largest spread in the value of peak droplet size. However, it is clear that the distributions show a high degree of overlap, and possess a well defined peak. If we consider all of our data (not just those shown in Fig. 7), and we use the standard deviation of the lognormal distribution to define its width, we find that the average ratio of the distributions width to the peak droplet size is 0.67. The variation seen in the distributions is likely due to small differences in the fluid sample from day to day, for example, differences in surface cleanliness. The differences in the distributions are not an artifact of the data analysis.

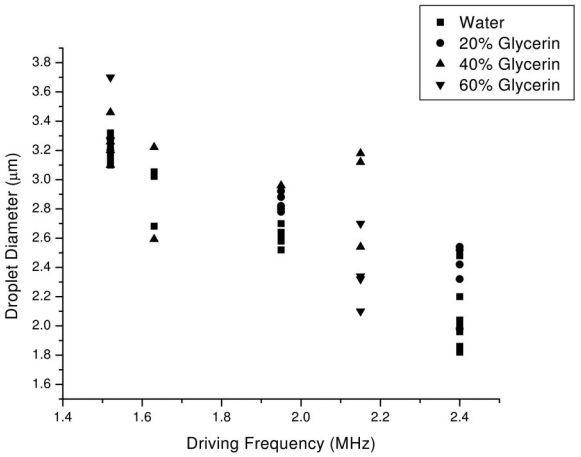

FIG. 6. Droplet diameter data. Droplet diameters for water–glycerin mixtures are shown for driving frequencies of 1.52–2.42 MHz. Droplet diameters were observed over a range of 1.82–3.70 μm.

Droplet diameters and uncertainties for all sets of fluids and driving frequencies are shown in Table I. The values quoted are the averages of the data points shown in Fig. 6, and the uncertainties are the standard deviation of the mean of each set of data points. The droplet data were then converted to nondimensional form using Eq. (1). Figure 8 shows a plot of the nondimensional diameter D versus the nondimensional driving frequency Ω. A two-parameter least-squares fit of these data yielded a power law relationship between D and Ω of -0.66 ± 0.01. Recall that the nondimensional power law in the inviscid regime was given by Eq. (2) to be $-2/3$, and that in the viscous regime, a $-1/2$ scaling law is expected. The fitted slope strongly indicates that the nondimensional data lie within the inviscid

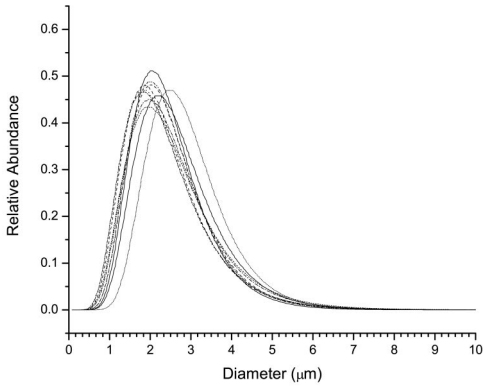

FIG. 7. Lognormal distributions. The distribution of droplet sizes resulting from driving pure water at 2.42. MHz. The distributions represent the best fits of the various data sets to a lognormal distribution. The distributions are well peaked and the width to peak droplet size ratio has an average of 0.71.

TABLE I. Droplet data. The droplet data sets are listed here, including the uncertainty, calculated as the standard deviation of the mean each dataset. Note that the uncertainties here are uncorrected for the measured variation in temperature; consequently they act as an upper bound.

Substance	Frequency	Diameter (μm)	Uncertainty (μm)
Water	1.52 MHz	3.20	0.03
Water	1.63 MHz	2.92	0.12
Water	1.95 MHz	2.61	0.03
Water	2.4 MHz	2.02	0.06
20% Glycerin	1.52 MHz	3.24	0.04
20% Glycerin	1.95 MHz	2.84	0.03
20% Glycerin	2.4 MHz	2.36	0.10
40% Glycerin	1.52 MHz	3.26	0.06
40% Glycerin	1.63 MHz	2.91	0.31
40% Glycerin	1.95 MHz	2.96	[a]
40% Glycerin	2.15 MHz	3.04	0.13
60% Glycerin	1.52 MHz	3.70	[a]
60% Glycerin	2.15 MHz	2.30	0.12

[a]For the sets with only one data point, the uncertainty cannot be computed.

regime, as expected. Figure 9 shows our data overlaid on a plot of the theoretical scaling laws in both the inviscid and the viscous regimes. Notice that the data match the inviscid scaling law all the way to the transition point between the two regimes. This fit gives a value of the diameter to wavelength ratio of $c=0.35\pm0.03$, which agrees closely with a literature value of 0.34.[10]

B. Droplet density measurement

The density of an aerosol can be determined by measuring the fractional transmission of light through a known length of the aerosol. As a laser beam propagates through an aerosol, the droplets it encounters scatter light into all angles, effectively reducing the intensity along the beam axis. The fractional transmission of a beam through a monodisperse aerosol of length L consisting of droplets of radius r is given by

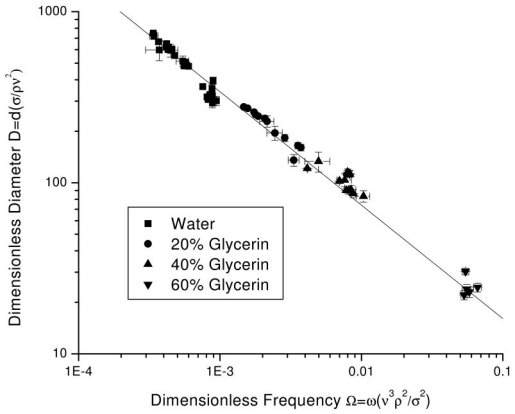

FIG. 8. Nondimensional droplet diameter data. The solid line is a two-parameter least-squares fit of Eq. (2) using the fitted peak droplet diameters of each of the 58 aerosols that were sized. The fit indicates a power-law relationship of -0.66 ± 0.01 and a diameter to wavelength ratio of $c=0.35\pm0.03$. The value of χ^2 for this fit is 16.3. Uncertainties were determined using the observed temperature variation that occurred during each dataset and the variation in d_{peak} that was observed over repeated (typically, five) trials with the same aerosol.

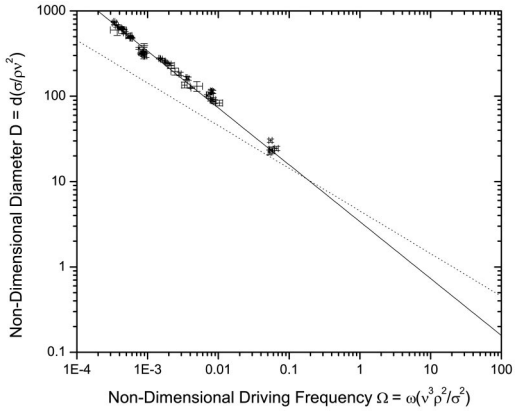

FIG. 9. Nondimensional droplet diameter data. The nondimensional data shown with the theoretical scaling laws predicted by Eqs. (2) and (3). To generate the theory curves, a diameter to wavelength ratio of $c=0.34$ was used. The inviscid regime has been well characterized, and it is clear that the theoretically expected inviscid scaling law is obeyed even for MHz-driving frequencies and micron-diameter droplets.

$$\frac{I}{I_0}=\exp[-NQ_{\text{sca}}\pi r^2 L], \tag{15}$$

where N is the number density and Q_{sca} is the scattering efficiency factor.[29]

Density data were taken for aerosols produced from pure water using the 2.42 MHz piezoelectric oscillator. A droplet sizing measurement yielded a peak droplet radius of 0.83 μm. The average transmission for this aerosol was found to be

$$\frac{I}{I_0}=0.982\pm0.006. \tag{16}$$

The length L of the aerosol illuminated by the laser was measured to be approximately 1 mm. From these measurements, the density can be determined using Eq. (15), and is found to be

$$N\approx 4\times10^6 \text{ droplets/cm}^3. \tag{17}$$

Next, the atomic density of an aerosol is given by[31]

$$N_{\text{atomic}}=\frac{n_a N\rho\,\frac{4}{3}\pi r^3}{mu}, \tag{18}$$

where n_a is the number of atoms per molecule, ρ is the fluid density, m is the molecular mass, and u is the molecular mass unit. For the same water aerosol, $\rho\approx1000$ kg/m^3, $r=0.83\times10^{-6}$ m, $m=18$ amu, $u=1.66\times10^{-27}$ kg/amu, $N=4\times10^{12}$ droplets/m^3, and $n_a=3$ for H_2O. Thus, the atomic density for this aerosol is

$$N_{\text{atomic}}\approx10^{18} \text{ atoms/cm}^3. \tag{19}$$

Fusion events have been observed in experiments involving deuterium clusters with average atomic density of 1.5×10^{19} atoms/cm^3.[3] Although the measured value of N_{atomic} is about 1 order of magnitude smaller than this, the measurement was made on an aerosol being blown in front of the laser by compressed air (see Fig. 4). This delivery process somewhat dilutes the aerosol, and if instead the

droplets are allowed to collect inside the aerosol container, then much higher atomic densities should be easily achievable. Thus, the estimate of N_{atomic} performed here indicates that this droplet source is capable of providing the high atomic densities that are necessary for laser fusion experiments.

V. CONCLUSION

In this paper we have used ultrasonic atomization in the MHz frequency range to generate aerosols of droplets at the micron scale, and Mie scattering methods to accurately measure the droplet size distribution. We have shown that the droplet diameter follows an inviscid scaling law at length-scales several orders of magnitude below previous experimental investigations. This is in contrast with results of Goodridge,[12] whose work suggests that viscous effects in the threshold forcing amplitude for droplet ejection occur at a dimensionless frequency 4 orders of magnitude smaller. This may be partially explained by considering linear instability of Faraday waves with weak dissipation, for which the most unstable wavelength (a proxy for droplet diameter) is independent of viscosity at leading order, while the threshold instability amplitude is proportional to viscosity.

Our comparison of the experimentally measured droplet size with the most unstable wavelength at the onset of Faraday instability, confirms a previous prediction by Lang[10] for the ratio of these two lengths. In addition, our analysis of the Faraday instability suggests that viscous effects should become relevant at a dimensionless frequency only twice our current maximum. At present we are investigating this regime; curiously, our initial results suggest that significantly larger piezo forcing amplitudes are necessary to atomize droplets in the viscous regime.

Due to their relatively large droplet size, the aerosols we currently produce are only marginally useful for the aforementioned fusion research. However, by moving to higher driving frequencies and lowering the fluid's surface tension (e.g., by mixing water with ethanol, or adding surfactants), we should be able to reduce droplet sizes to a more relevant range.

ACKNOWLEDGMENTS

We thank T. Ditmire for useful conversations, and the referees for their careful reading of the manuscript and their insightful criticism. Parts of this research were supported by the Beckman Research Fund at Harvey Mudd College. Acknowledgement is made to the Donors of The Petroleum Research Fund administered by the American Chemical Society, for partial support of this research, and for support by an award from the Research Corporation.

[1] J. J. Duderstadt and G. A. Moses, *Inertial Confinement Fusion* (Wiley, New York, 1982).
[2] T. J. Murphy, J. L. Jimerson, R. R. Berggren, J. R. Faulkner, J. A. Oertel, and P. J. Walsh, "Neutron time-of-flight and emission time diagnostics for the National Ignition Facility," Rev. Sci. Instrum. **72**, 850 (2001).
[3] T. Ditmire, J. Zweiback, V. P. Yamovsky, T. E. Cowan, G. Hays, and K. B. Wharton, "Nuclear fusion in gases of deuterium clusters heated with a femtosecond laser," Phys. Plasmas **7**, 1993 (2000).
[4] T. Ditmire, J. Zweiback, V. P. Yamovsky, T. E. Cowan, G. Hays, and K. B. Wharton, "Nuclear fusion from explosions of femtosecond laser-heated deuterium clusters," Nature (London) **398**, 489 (1999).
[5] T. Ditmire, J. Zweiback, V. P. Yamovsky, T. E. Cowan, G. Hays, and K. B. Wharton, "Nuclear fusion in gases of deuterium clusters heated with a femtosecond laser," Phys. Plasmas **7**, 1993 (2000).
[6] T. D. Donnelly, M. Rust, I. Weiner, M. Allen, R. A. Smith, C. A. Steinke, S. Wilks, J. Zweiback, T. E. Cowan, and T. Ditmire, "Hard x-ray and hot electron production from intense laser irradiation of wavelength scale particles," J. Phys. B **34**, L313 (2001).
[7] T. Ditmire, T. D. Donnelly, A. M. Rubenchik, R. W. Falcone, and M. D. Perry, "The interaction of intense laser pulses with atomic clusters," Phys. Rev. A **53**, 3379 (1996).
[8] M. Dobre and L. Bolle, "Theoretical prediction of ultrasonic spray characteristics using the maximum entropy formalism," Proceedings ILASS-Europe 98, Manchester, England, 1998, pp. 7–12.
[9] B. T. Forrest, "Modeling small droplet ejection from a fluid due to capillary waves," Senior thesis, Harvey Mudd College, Claremont, California, 2002.
[10] R. J. Lang, "Ultrasonic atomization of liquids," J. Acoust. Soc. Am. **34**, 6 (1962).
[11] D. Sindayihebura, M. Dobre, and L. Bolle, "Experimental study of thin liquid film ultrasonic atomization," Proceedings ExHFT-4, Brussels, Belgium, 1997.
[12] C. L. Goodridge, W. T. Shi, H. G. E. Hentschel, and D. P. Lathrop, "Viscous effects in droplet-ejecting capillary waves," Phys. Rev. E **56**, 472 (1997).
[13] I. Weiner, M. Rust, and T. D. Donnelly, "Particle size determination: An undergraduate lab in Mie scattering," Am. J. Phys. **69**, 129 (2001).
[14] J. Miles and D. Henderson, "Parametrically forced surface waves," Annu. Rev. Fluid Mech. **22**, 143 (1990).
[15] M. Faraday, "On the forms and states assumed by fluids in contact with vibrating elastic surfaces," Philos. Trans. R. Soc. London **52**, 319 (1831).
[16] T. B. Benjamin and F. Ursell, "The stability of a plane free surface of a liquid in vertical periodic motion," Proc. R. Soc. London, Ser. A **225**, 505 (1954).
[17] K. Kumar and L. S. Tuckerman, "Parametric instability of the interface between two fluids," J. Fluid Mech. **279**, 49 (1994).
[18] J. Beyer and R. Friedrich, "Faraday instability: Linear analysis for viscous fluids," Phys. Rev. E **51**, 1162 (1995).
[19] J. Bechhoefer, V. Ego, S. Manneville, and B. Johnson, "An experimental study of the onset of parametrically pumped surface waves in viscous fluids," J. Fluid Mech. **288**, 325 (1995).
[20] O. Lioubashevski, J. Fineberg, and L. S. Tuckerman, "Scaling of the transition to parametrically driven surface waves in highly dissipative systems," Phys. Rev. E **55**, R3832 (1997).
[21] E. Cerda and E. Tirapegui, "Faraday's instability for viscous fluids," Phys. Rev. Lett. **78**, 859 (1997).
[22] E. A. Cerda and E. L. Tirapegui, "Faraday's instability in viscous fluid," J. Fluid Mech. **368**, 195 (1998).
[23] S. Kumar, "Mechanism for the Faraday instability in viscous liquids," Phys. Rev. E **62**, 1416 (2000).
[24] J. Miles, "On Faraday resonance of a viscous liquid," J. Fluid Mech. **395**, 321 (1999).
[25] C. L. Goodridge, W. T. Shi, and D. P. Lathrop, "Threshold dynamics of singular gravity-capillary waves," Phys. Rev. Lett. **76**, 1824 (1996).
[26] A. J. James, M. K. Smith, and A. Glezer, "Vibration-induced drop atomization and the numerical simulation of low-frequency single-droplet ejection," J. Fluid Mech. **476**, 29 (2003).
[27] A. J. James, B. Vukasinovic, M. K. Smith, and A. Glezer, "Vibration-induced drop atomization and bursting," J. Fluid Mech. **476**, 1 (2003).
[28] W. Wiscombe, "Improved Mie scattering algorithms," Appl. Opt. **19**, 1505 (1980).
[29] M. Kerker, *The Scattering of Light and Other Electromagnetic Radiation* (Academic, New York, 1969).
[30] P. R. Bevington and D. K. Robinson, *Data Reduction and Error Analysis for the Physical Sciences*, 2nd ed. (McGraw–Hill, Boston, 1992).
[31] L. C. Mountford, R. A. Smith, and M. H. R. Hutchinson, "Characterization of a sub-micron liquid spray for laser-plasma x-ray generation," Rev. Sci. Instrum. **69**, 3780 (1998).